Original Article

Breaking diffraction limit of lateral resolution in optical coherence tomography

Benquan Wang[1], Rongwen Lu[1], Qiuxiang Zhang[1], Xincheng Yao[1,2,3]

[1]Department of Biomedical Engineering, University of Alabama at Birmingham, Birmingham, AL 35294, USA; [2]Department of Vision Sciences, University of Alabama at Birmingham, Birmingham, AL 35294, USA; [3]Vision Science Research Center, University of Alabama at Birmingham, Birmingham, AL 35294, USA

Corresponding to: Xincheng Yao, PhD. 390B Volker Hall, 1670 University Blvd, Birmingham, AL 35294, USA. Email: xcy@uab.edu.

Abstract: Quantitative imaging of biomedical specimens is essential in biomedical study and diagnosis. Given excellent capability in three-dimensional (3D) imaging, optical coherence tomography (OCT) has been extensively used in ophthalmic imaging, vascular medicine, dermatological study, etc. Lateral resolution of the OCT is light diffraction limited, which precludes the feasibility of quantitative assessment of individual cells. In this paper, we demonstrated the feasibility of breaking diffraction-limit in OCT imaging through virtually structured detection (VSD). OCT examination of optical resolution target verified resolution doubling in the VSD based OCT imaging. Super-resolution OCT identification of individual frog photoreceptors was demonstrated to verify the potential of resolution enhancement in retinal imaging. We anticipate that further development of the VSD based OCT promises an easy, low cost strategy to achieve sub-cellular resolution tomography of the retina and other biological systems.

Keywords: Optical coherence tomography (OCT); retina; three-dimensional imaging

Submitted Sep 21, 2013. Accepted for publication Oct 29, 2013.
doi: 10.3978/j.issn.2223-4292.2013.10.03
Scan to your mobile device or view this article at: http://www.amepc.org/qims/article/view/2872/3827

Introduction

High resolution imaging is important for accurate characterization of pathological abnormalities of biomedical specimens. Given the excellent axial resolution in three-dimensional (3D) imaging (1-4), optical coherence tomography (OCT) has been extensively used in retinal examination, vascular medicine (5,6), and dermatological study (7,8), etc. Axial resolution of the OCT is dependent on the spectral bandwidth of the selected light sources; while lateral resolution of the OCT is diffraction limited (9). In coordination with careful optical designs (10,11) and adaptive optics (AO) (12), OCT imaging can be implemented at diffraction limit (13). However, quantitative OCT imaging is till challenging due to the resolution limit to resolve individual cells or even sub-cellular structures. In principle, the resolution can be improved by increasing the numerical aperture (NA) of optical systems. However, the working distance, i.e., imaging depth, of an optical instrument can be dramatically reduced as increasing NA. Moreover, the available NA is not changeable in some situations. For example, retinal imaging is limited by optical quality, including the NA which has the maximum ~0.25, of the eye. Therefore, alternative strategies have to be considered for resolution improvement. Several numerical strategies such as deconvolution algorithms (14-17) and digital focusing (18) have been explored to improve the lateral resolution of OCT. Although digital deconvolution has the potential in theory to exceed the diffraction limit for OCT imaging (15-17), the accurate estimation of the point spread function (PSF) of the OCT system, which is required for deconvolution, is practically challenging. So far, a feasible strategy of super-resolution OCT imaging is still yet to be demonstrated.

Structured illumination microscopy (SIM) has been demonstrated to break through optical resolution limited by light diffraction. However, spatially structured wide

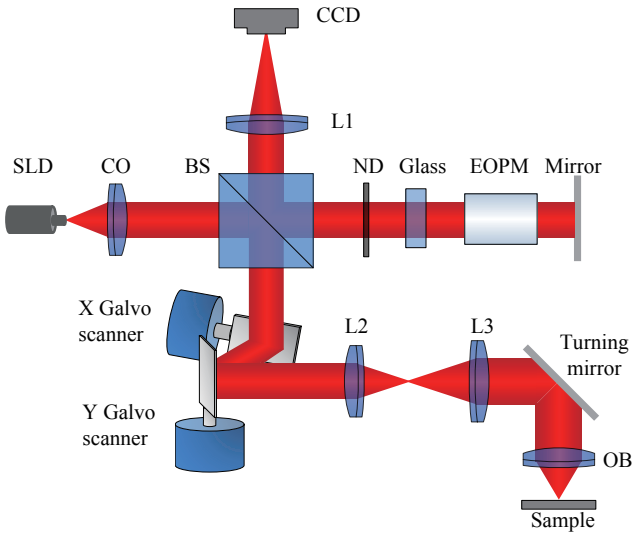

Figure 1 Diagram of the super-resolution OCT. OCT, optical coherence tomography; SLD, superluminescent diode, wavelength λ =830 nm, band width Δλ =60 nm; CO, collimator; BS, beam splitter; L1-L3, lenses, focal lengths of lenses L1-L3 are 200, 40 and 150 mm, respectively; ND, neutral density filter; EOPM, electro-optic phase modulator; OB, objective (5×, 0.1 NA). The lateral resolution of the system is 5 μm and the axial resolution is 4 μm.

field illumination is not suitable for scanning laser imaging modalities, such as OCT. In theory, an alternative strategy to the SIM is to combine spatial and temporal modulations, either by spatiotemporal modulation of the scanning laser profile (in the illumination path) or the recording light profile (in the detection path) (19). However, physical implementation of the illumination/detection modulation is difficult. So far, experimental validation of the proposed spatiotemporal modulation is not yet demonstrated. We recently demonstrated a virtually structured detection (VSD) based super-resolution scanning laser microscopy (SLM) to achieve resolution doubling (20). Without the complexity of structured illumination, VSD provides an easy, low-cost and phase-artifact free strategy to achieve super-resolution imaging. The purpose of this study is to demonstrate the feasibility of breaking diffraction-limited resolution in OCT imaging through VSD. OCT examination of optical resolution target verified resolution enhancement in the VSD based imaging. Super-resolution OCT identification of individual frog photoreceptors was validated to demonstrate the potential of resolution enhancement in retinal imaging. We anticipate that further development of the VSD based OCT can provide an easy, low cost strategy to achieve sub-cellular resolution tomography of the retina and other biological systems.

Materials and methods

Experimental setup

Figure 1 shows the diagram of the VSD based super-resolution OCT. A near infrared superluminescent diode (SLD-351, Superlum) with a center wavelength λ =830 nm and band width Δλ =60 nm was used to illuminate the sample. A dual-axis galvo (GVS002, Thorlabs) was used to scan the focused illuminating light across the sample in a raster pattern and descan light reflected from sample to the light detector. We used a two-dimensional (2D) digital camera (Pike F-032B, Allied Vision Technologies) to replace the single element sensor in conventional time-domain OCT. In the reference arm, neutral density filters were applied to adjust light intensity. A glass block was inserted into the reference arm to compensate for optical dispersion (21) of the electro-optic phase modulator (EOPM, Model 350-50, Conoptics), which was employed to introduce rapid vibration free phase modulation for OCT reconstruction (22). Briefly, EOPM shifted reference beam light phase by 0, π/2, π and 3π/2 at each scanning position. Four corresponding interference patterns were recorded at each scanning position for OCT reconstruction. The axial resolution of the system was ~4 μm (0.44 $\lambda^2/n\Delta\lambda$, where n was the refractive index of the sample, ~1.4). With a 0.1 NA 5× objective, lateral resolution of conventional OCT was theoretically estimated at ~5 μm (0.61 λ/NA). In theory, the VSD can improve the resolution by a factor of 2 (19,20,23). A virtual pinhole (two times of the Airy disc diameter) was applied during reconstruction.

Principle of the VSD based OCT

For simplicity, formulas will be written in one-dimension. During the OCT recording, the reference mirror was adjusted to a position where the zero delay plane is superimposed with the focal plane. First, the standard four-frame phase-shifting algorithm is applied to retrieve OCT images (24). By ignoring optical magnification, the interference pattern (in X direction) recorded by the camera at a given scanning position x_0 is

$$I_i(x,x_0) = I_S(x,x_0) + I_R(x) + 2\sqrt{I_S(x,x_0)I_R(x)}\cos[\theta(x,x_0)+\delta_i] \quad [1]$$

where I_S is the intensity distribution of light reflected from sample, I_R is the intensity distribution of light reflected from mirror in the reference arm, θ is the time-invariant phase difference distribution between the sampling arm and the reference arm, i =1,2,3,4 and δ_i is the phase modulation item:

$$\delta_i = (i-1)\pi/2 \quad [2]$$

According to the standard four-frame phase-shifting algorithm (24), we will have

$$I_S(x,x_0) = \frac{[I_1(x,x_0)-I_3(x,x_0)]^2+[I_2(x,x_0)-I_4(x,x_0)]^2}{I_R(x)} \quad [3]$$

If we assume the reference intensity profile is spatially invariant within the virtual pinhole:

$$I_R(x) = c \quad [4]$$

and constant coefficients are ignored, the Eq. [3] can be simplified as:

$$I_S(x,x_0) = [I_1(x,x_0)-I_3(x,x_0)]^2+[I_2(x,x_0)-I_4(x,x_0)]^2 \quad [5]$$

The second step is to apply VSD to break through diffraction limit of lateral resolution. Details of VSD have been reported in our recent publication (20). Briefly, a digital sinusoidal mask $m(x)$ is applied to multiply with the OCT profile map:

$$I_{mul}(x,x_0) = I_S(x,x_0)m(x) \quad [6]$$

The spatial integral of Eq. [6] yields:

$$\begin{aligned} p(x_0) &= \int I_{mul}(x,x_0)dx \\ &= h_{il}(x_0)\otimes\{s(x_0)[h_{de}(x_0)\otimes m(x_0)]\} \end{aligned} \quad [7]$$

where h_{il} and h_{de} are PSFs of the illumination beam and detection beam, respectively, and s is the reflectance ratio of the sample. Fourier transforming Eq. [7] yields:

$$\tilde{p}(f_x) = \tilde{h}_{il}(f_x)\{\tilde{s}(f_x)\otimes[\tilde{h}_{de}(f_x)\tilde{m}(f_x)]\} \quad [8]$$

We can see that if the carrier frequency of $\tilde{m}$ is smaller than the cutoff frequency of $\tilde{h}_{de}$, the convolution in Eq. [8] can shift the high frequency of the sample toward the lower frequency to pass through $\tilde{h}_{il}$, thus to break through diffraction limited resolution.

Sample preparation

We used a standard optical resolution target (USAF 1951 1X, Edmond) and freshly isolated frog (Rana Pipiens) for experimental validation of the proposed VSD based OCT system. The optical resolution target provided a simple sample for technical validation of the OCT resolution. In contrast to simple optical target, frog retina had relatively complex 3D structures. The diameter of frog photoreceptor rod was 5-8 μm and that of cone was about 1-3 μm (25,26), which provided an excellent model to test OCT resolution before (5 μm) and after (2.5 μm) VSD data processing. All animal handling procedure was approved by the Institutional Animal Care and Use Committee of the University of Alabama at Birmingham. Frog used for preparing freshly isolated retina was firstly euthanized by rapid decapitation and double pithing. Then eyeball was detached and moved to Ringer's solution [containing (27) in mmol/L: 110 NaCl, 2.5 KCl, 1.6 $MgCl_2$, 1.0 $CaCl_2$, 22 $NaHCO_3$, and 10 D-glucose]. After hemisecting the eyeball with fine scissors, lens was removed and the retina was separated from the eyecup. Dissected retina was then moved to a chamber filled with Ringer's solution for image recording. All procedure was conducted in a dark room illuminated with dim red light.

Results

Super-resolution OCT imaging of optical resolution target

Figure 2 compares conventional OCT image and the VSD based OCT image of the optical resolution target. The smallest grating of the optical resolution target had a period of 4.4 μm. Since the lateral resolution of the conventional OCT system was 5 μm, the smallest grating could not be resolved by conventional OCT as indicated by the white arrow in *Figure 2A*. Moreover, it was difficult for conventional OCT to differentiate the second smallest grating which has a period of 4.9 μm (blue arrow in *Figure 2A*). In contrast, the VSD based OCT was capable of resolving both the smallest grating (white arrow in *Figure 2B*) and the second smallest grating (blue arrow in *Figure 2B*). The normalized intensity profile in *Figure 2C* confirmed the resolution enhancement of the VSD based OCT. Three clear bumps corresponding to the second smallest grating (blue dashed rectangle in *Figure 2C*) and three bumps corresponding to the smallest grating (white dashed rectangle in *Figure 2C*) manifested themselves more clearly after VSD reconstruction.

Super-resolution OCT imaging of freshly isolated retina

After we tested super-resolution OCT using the optical

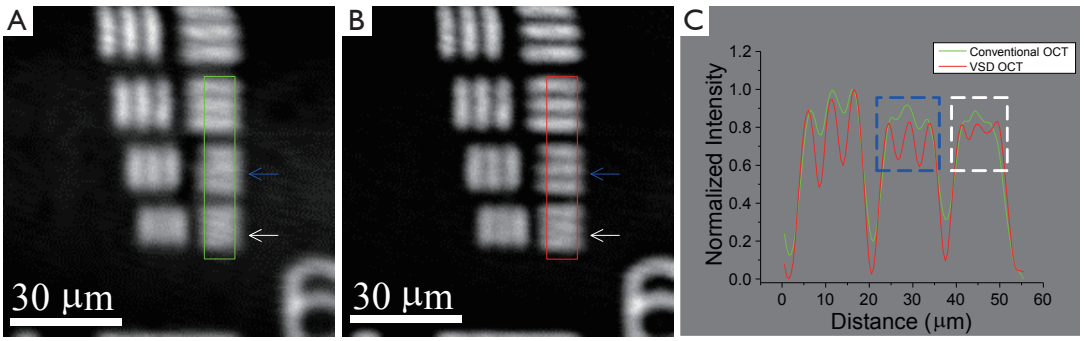

Figure 2 VSD based super-resolution OCT imaging of optical resolution target. (A) Image of optical resolution target acquired by conventional OCT; (B) Image of optical resolution target acquired by the VSD based super-resolution OCT; (C) Normalized intensity profiles of optical resolution target. The green curve was the normalized intensity profile from top to bottom of the area specified by the green rectangle in (A). The red curve was the normalized intensity profile from top to bottom of the area specified by the red rectangle in (B). Abbreviations: VSD, virtually structured detection; OCT, optical coherence tomography.

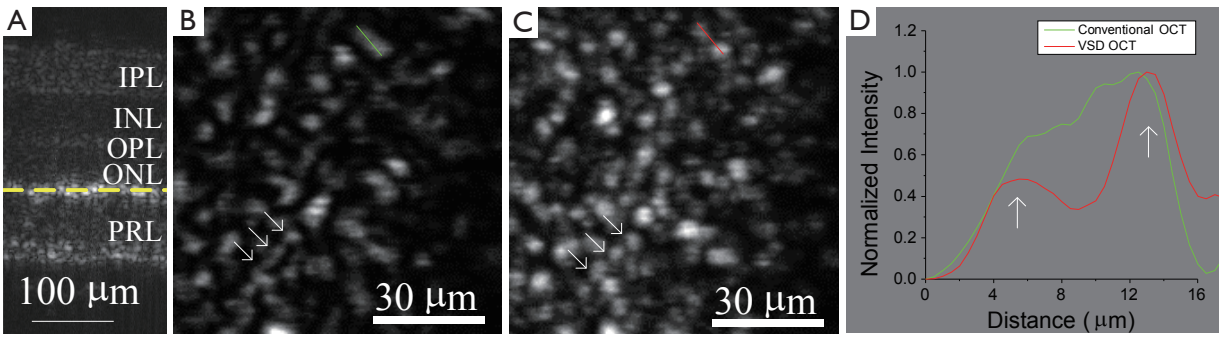

Figure 3 VSD based super-resolution OCT imaging of freshly isolated retina. (A) B-scan of isolated frog retina. Different retinal layers can be observed. From top to bottom they are: IPL, INL, OPL, ONL and PRL. The yellow dashed line indicated the position where enface OCT images were acquired; (B) Enface image of isolated frog retina acquired by conventional OCT; (C) Enface image of isolated frog retina acquired by the VSD based super-resolution OCT; (D) Normalized intensity profiles of retina. The green curve was the normalized intensity profile along the green line in (B). The red curve was the normalized intensity profile along the red line in (C). Abbreviations: VSD, virtually structured detection; OCT, optical coherence tomography; IPL, inner plexiform layer; INL, inner nuclear layer; OPL, outer plexiform layer; ONL, outer nuclear layer; PRL, photoreceptor layer.

resolution target, we implemented super-resolution OCT imaging of freshly isolated frog retina. *Figure 3A* shows a cross-section image of freshly isolated frog retina acquired by conventional OCT. With ~4 μm axial resolution, we could clearly see retinal layer structure which consisted of inner plexiform layer (IPL), inner nuclear layer (INL), outer plexiform layer (OPL), outer nuclear layer (ONL) and photoreceptor layer (PRL). Enface images were acquired at the inner segment of PRL (yellow dashed line in *Figure 3A*) which rendered strong OCT signal and rich structure details. Comparing *Figure 3B* to *Figure 3C*, we can see that in *Figure 3C* more cellular structures could be observed. For example, three individual photoreceptors could be identified (three white arrows in *Figure 3C*), while only a single blur structure could be visualized at the same area in *Figure 3B*. Resolution enhancement was also confirmed by comparing light intensity profiles. The green and red curves in *Figure 3D* corresponded to normalized intensity profiles along the green line in *Figure 3B* and the red line in *Figure 3C*, respectively. Two individual cells were separated on the red curve (white arrows in *Figure 3D*), while they merged together on the green curve.

Discussion

In summary, we demonstrated that VSD can be implanted

in OCT imaging to break through the diffraction limit. OCT imaging of optical resolution target (*Figure 2*) and frog retinal photoreceptors (*Figure 3*) showed noticeable resolution improvement. Detailed structures that were not identified in conventional OCT images could be readily resolved in super-resolution OCT images through the VSD. Although the VSD based method can be implemented in an imaging system with a high magnification objective, we selected a relatively low magnification objective (5×) in this study for technical validation of super-resolution imaging of frog photoreceptors. Since frog retina consists of photoreceptors with variable diameters (rods: ~5-8 μm; cones: ~1-3 μm) (26,27), it provided an excellent preparation to evaluate the OCT resolution before (5 μm) and after (2.5 μm) VSD data processing.

During VSD reconstruction, the virtual pinhole size was set to two times of the Airy disc diameter. Within the virtual pinhole, we assumed the intensity profile of the light from the reference arm was uniform, as shown in Eq. [4]. However, the actual light intensity attenuated away from the center and became weak at the edge of the virtual pinhole. In other words, the virtual pinhole was truncated by the reference light profile. Therefore, the effective pinhole size became smaller. A smaller confocal pinhole (i.e., <1 Airy disc diameter) can in theory improve the lateral resolution in a confocal system (28). However, with a smaller effective pinhole size, some information was lost for VSD reconstruction. One method to readily alleviate the attenuation of the reference light intensity is to insert an aperture at the reference beam. Since the reference light beam size is smaller, the diffraction map, which is the Fourier Transform of the parallel reference light, becomes larger. Therefore, the diffraction profile will become more uniform at the center. An alternative solution is to use a fiber splitter and feed one port to the sampling arm and the other to the reference arm. With this configuration, it is possible to focus the sampling light beam to the camera while maintaining the parallelism of the reference light beam.

The imaging speed of our current super-resolution OCT is relatively slow (40 s per frame). The VSD imposes a spatially resolved detector to record the diffraction profile of each scanning position, which is time-consuming and infeasible for *in vivo* retinal imaging due to possible eye movements during the recording. Currently, we are integrating a microlens array (MLA) based multifocal scanning system (29) to improve the speed of super-resolution OCT imaging. We anticipate that further development of the VSD based OCT can provide a practical strategy to achieve super-resolution in *in vivo* OCT imaging of retinal structures.

Acknowledgements

This research is supported in part by NSF CBET-1055889, NIH R21 EB012264, and UASOM I3 Pilot Award.
Disclosure: The authors declare no conflict of interest.

References

1. Huang D, Swanson EA, Lin CP, et al. Optical coherence tomography. Science 1991;254:1178-81.
2. Hee MR, Izatt JA, Swanson EA, et al. Optical coherence tomography of the human retina. Arch Ophthalmol 1995;113:325-32.
3. Swanson EA, Izatt JA, Hee MR, et al. In vivo retinal imaging by optical coherence tomography. Opt Lett 1993;18:1864-6.
4. Baumal CR. Clinical applications of optical coherence tomography. Curr Opin Ophthalmol 1999;10:182-8.
5. Qin J, Jiang J, An L, et al. In vivo volumetric imaging of microcirculation within human skin under psoriatic conditions using optical microangiography. Lasers Surg Med 2011;43:122-9.
6. Wang RK, Jacques SL, Ma Z, et al. Three dimensional optical angiography. Opt Express 2007;15:4083-97.
7. Gambichler T, Jaedicke V, Terras S. Optical coherence tomography in dermatology: technical and clinical aspects. Arch Dermatol Res 2011;303:457-73.
8. Saxer CE, de Boer JF, Park BH, et al. High-speed fiber based polarization-sensitive optical coherence tomography of in vivo human skin. Opt Lett 2000;25:1355-7.
9. Fernández E, Drexler W. Influence of ocular chromatic aberration and pupil size on transverse resolution in ophthalmic adaptive optics optical coherence tomography. Opt Express 2005;13:8184-97.
10. Fernández EJ, Unterhuber A, Povazay B, et al. Chromatic aberration correction of the human eye for retinal imaging in the near infrared. Opt Express 2006;14:6213-25.
11. Zawadzki RJ, Cense B, Zhang Y, et al. Ultrahigh-resolution optical coherence tomography with monochromatic and chromatic aberration correction. Opt Express 2008;16:8126-43.
12. Liang J, Williams DR, Miller DT. Supernormal vision and high-resolution retinal imaging through adaptive optics. J Opt Soc Am A Opt Image Sci Vis 1997;14:2884-92.

13. Zhang Y, Rha J, Jonnal R, et al. Adaptive optics parallel spectral domain optical coherence tomography for imaging the living retina. Opt Express 2005;13:4792-811.
14. Ralston TS, Marks DL, Carney PS, et al. Inverse scattering for optical coherence tomography. J Opt Soc Am A Opt Image Sci Vis 2006;23:1027-37.
15. Yasuno Y, Sugisaka J, Sando Y, et al. Non-iterative numerical method for laterally superresolving Fourier domain optical coherence tomography. Opt Express 2006;14:1006-20.
16. Liu Y, Liang Y, Mu G, et al. Deconvolution methods for image deblurring in optical coherence tomography. J Opt Soc Am A Opt Image Sci Vis 2009;26:72-7.
17. Woolliams PD, Ferguson RA, Hart C, et al. Spatially deconvolved optical coherence tomography. Appl Opt 2010;49:2014-21.
18. Yu L, Rao B, Zhang J, et al. Improved lateral resolution in optical coherence tomography by digital focusing using two-dimensional numerical diffraction method. Opt Express 2007;15:7634-41.
19. Lu J, Min W, Conchello JA, et al. Super-resolution laser scanning microscopy through spatiotemporal modulation. Nano Lett 2009;9:3883-9.
20. Lu RW, Wang BQ, Zhang QX, et al. Super-resolution scanning laser microscopy through virtually structured detection. Biomed Opt Express 2013;4:1673-82.
21. Yao XC, Yamauchi A, Perry B, et al. Rapid optical coherence tomography and recording functional scattering changes from activated frog retina. Appl Opt 2005;44:2019-23.
22. Lu RW, Curcio CA, Zhang Y, et al. Investigation of the hyper-reflective inner/outer segment band in optical coherence tomography of living frog retina. J Biomed Opt 2012;17:060504.
23. Gustafsson MG. Surpassing the lateral resolution limit by a factor of two using structured illumination microscopy. J Microsc 2000;198:82-7.
24. Huntley JM, Saldner H. Temporal phase-unwrapping algorithm for automated interferogram analysis. Appl Opt 1993;32:3047-52.
25. Liebman PA, Entine G. Visual pigments of frog and tadpole (Rana pipiens). Vision Res 1968;8:761-75.
26. Nilsson SE. An electron microscopic classification of the retinal receptors of the leopard frog (rana pipiens). J Ultrastruct Res 1964;10:390-416.
27. Meister M, Pine J, Baylor DA. Multi-neuronal signals from the retina: acquisition and analysis. J Neurosci Methods 1994;51:95-106.
28. Wilson T, Carlini AR. Size of the detector in confocal imaging systems. Opt Lett 1987;12:227-9.
29. Zhang QX, Wang JY, Liu L, et al. Microlens array recording of localized retinal responses. Opt Lett 2010;35:3838-40.

Cite this article as: Wang B, Lu R, Zhang Q, Yao X. Breaking diffraction limit of lateral resolution in optical coherence tomography. Quant Imaging Med Surg 2013;3(5):243-248. doi: 10.3978/j.issn.2223-4292.2013.10.03

